A wavelet algorithm for zoom-in tomography

Max Langer, Françoise Peyrin

A WAVELET ALGORITHM FOR ZOOM-IN TOMOGRAPHY

Max Langer, Françoise Peyrin

CREATIS, CNRS UMR 5220, INSERM U630, Université Lyon 1, INSA-Lyon, 69621 Villeurbanne, France
European Synchrotron Radiation Facility, 6 rue Jules Horowitz, 38043 Grenoble, France

ABSTRACT

In zoom-in tomography, the aim is to image a region of interest lying partially or fully within the imaged object, using a high resolution tomographic scan covering only the ROI, and a low resolution scan covering the whole object. We analyze the problem from a multiresolution point of view and propose an algorithm for combining the two data sets using the discrete wavelet transform and the Haar wavelet. We compare the proposed algorithm to a previously reported method that involves padding of the high resolution data with a supersampled version of the low resolution data, to zero padding and edge extension, using synthetic data sets. We show that the proposed algorithm is insensitive to offsets between the two data sets, but that it is slightly more sensitive to noise.

Index Terms— Computed tomography, reconstruction, multiresolution, wavelets, quantitative imaging

1. INTRODUCTION

There has recently been a surge in interest in local tomography reconstruction techniques. This problem is variously known as local tomography, region of interest (ROI) tomography, interior problem, and truncated projections and all refer to the case when the imaged object does not fit in the field of view of a tomographic imaging system (Fig. 1). This problem can arise in the clinical setting, e.g. due to obesity in a full body CT scan, but the recent increase in interest in this problem is mainly motivated by X-ray microscopy. As resolutions are pushed further and further toward the nanoscale, the available field-of-view (FOV) also decreases. Current Synchrotron Radiation (SR) μCT imaging setups, using high flux X-ray beam extracted from synchrotron sources, achieve pixel sizes down to ~0.3 μm. With a typical detector size of 2048×2048, this gives a FOV of ~0.6 mm. This makes it increasingly hard to manufacture samples that can be imaged in their entirety.

It is known that standard reconstruction from truncated projection yield different types of artifacts, usually visible as a discontinuity at the ROI periphery and cupping effect (shown in Fig. 3 & 6). This problem is especially important in quantitative imaging techniques such as SR-μCT. In this technique, the use of a monochromatic X-ray beam ensures that reconstructed gray-level values correspond to the local linear absorption coefficient (μ) distribution in the sample. The artifacts introduced by truncation, however, mainly affect the low frequency range of the reconstructed function, and the absolute value of the linear absorption coefficient is lost. Thus, truncation clearly destroys the quantitative aspect of SR-μCT.

Different cases of truncated projections problem can be discerned. The interior problem corresponds to the case where data acquisition is strictly limited to straight lines passing through the ROI (Fig. 1). In this case there is no unique solution to the problem [1]. However if some measurements in the external region are possible, different solutions have been proposed in literature, ranging from introduction of *a priori* knowledge [2], use of iterative algorithms [3], or wavelets [4-6]. In this paper, we focus on the problem of the reconstruction of a ROI from high resolution (HR) truncated projections knowing a set of low resolution (LR) non truncated projections. This case, sometimes called zoom-in tomography, appears to be less studied. This procedure was proposed already three decades ago [7,8], but was only recently applied to synchrotron imaging [9]. The algorithm essentially consists in recording two data sets at different magnifications, one global, LR acquisition where the object completely fits in the FOV, and one local, HR acquisition restricted to the desired ROI (Fig. 1). Such an acquisition can be achieved relatively easily in X-ray - μCT by acquiring data at different magnifications. In cone-beam CT, this can be obtained by changing the source to detector distance and in a 3D parallel beam CT setting by the use of interchangeable objective lenses with different magnification factors.

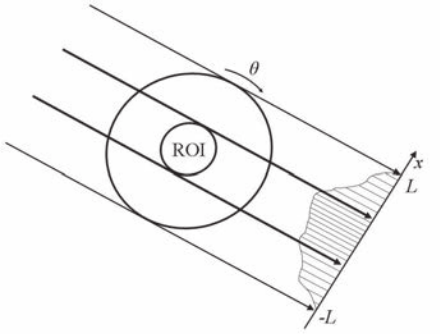

Fig. 1. Geometry of the parallel beam zoom-in tomography problem. It is desired to image a region of interest (ROI) partially or fully inside the imaged object at high resolution. However, a scan at lower resolution (keeping the same numbers of elements of the detector) where the object fits fully in the field of view is available.

In the previous works, the LR sinogram was supersampled to the same resolution as the HR sinogram. The data sets were registered and the corresponding part of the LR scan was then substituted for the HR data. This extended data set was then used as input to a tomographic reconstruction algorithm. The algorithm can be seen as an informed way of padding the HR acquisition data.

In this work, we propose a wavelet algorithm for reconstruction of zoom-in tomography data. Wavelets approaches have already been proposed in tomographic reconstruction and especially in the context of local tomography [4-6]. Knowledge of two data sets respectively at LR and HR fits well in the framework

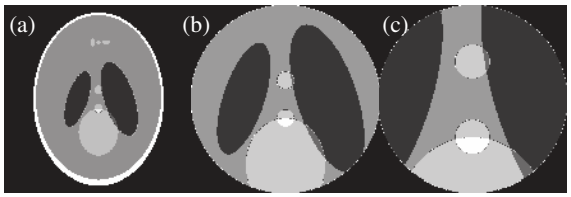

Fig. 2. Slices through direct digitizations of the 3D Shepp-Logan phantom (grayscale values in 32 bit float, [0 2], used in simulations, windowed to [0.99 1.04]. (a) Ideal reconstruction, 1x magnification (b) Ideal reconstruction, 2x magnification (c) Ideal reconstruction, 4x magnification.

of wavelets. We assume that the data magnifications are separated by a factor of power of two, to fit a dyadic wavelet transform. This is not necessary to enforce on the experimental level as this can be ensured by resampling the LR data.

Our approach is based on the observation that, ideally, if the HR data is acquired at twice the resolution of the LR data, the HR data should be identical to the LR data in the ROI, except that it contains wavelet coefficients at one higher scale. The algorithm then consists in performing a one level wavelet decomposition of the HR data, zero-padding the details to the same size as the LR data, and substituting the LR data for the approximation coefficients. If the LR and HR data are consistent on all other decomposition levels, the wavelet algorithm is actually identical to the substitution algorithm. The advantage of the wavelet algorithm is that if the lower scales are not consistent between the LR and HR data, it permits the use of the complete LR scan, which is always self-consistent. We apply the two algorithms to simulated data and show that they perform equally on noise-free and noisy data. We further demonstrate the improved robustness to inconsistencies between the two data sets by introducing a small offset in the HR data.

2. MULTIRESOLUTION ANALYSIS OF ZOOM-IN TOMOGRAPHY

Let f(x,y,z) be the 3D target function to be reconstructed. Its 2D parallel projection of angle θ when the object is rotated around the z-axis can be written as

$$p_\theta(r,z) = \int_{D_{\theta,r}} f(x,y,z)\,ds = \int f(r\cos\theta - s\sin\theta, r\sin\theta + s\sin\theta, z)\,ds \quad (1)$$

For a given z level, $p_\theta(r,z)$, $\theta \in [0,\pi[$ is the Radon transform of *f(x,y,z)*. The image can then be reconstructed with the filtered backprojection algorithm (FBP):

$$f(x,y,z) = \frac{1}{2}\int_0^\pi \hat{p}_\theta(x\cos\theta + y\sin\theta, z)\,d\theta \quad (2)$$

with

$$\hat{p}_\theta = (p_\theta *_r h)(r) \quad (3)$$

where $*_r$ denotes convolution with respect to r and

$$\Im_1 h(R) = |R|, \quad (4)$$

where $\Im_1$ denotes the 1D Fourier transform.

Zoom-in tomography is characterized by the acquisition of two distinct data sets: one HR scan strictly inside the ROI at the desired spatial resolution, and one LR scan where the imaged object fits completely in the FOV. If we suppose that the two data

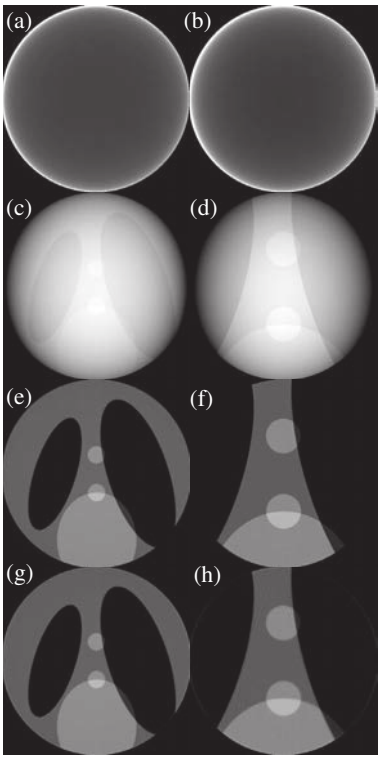

Fig. 3. Slices through the reconstructed volumes using noise free data, reconstructed with (a) x2 and (b) x4 magnification data with zero padding. Typical artifacts are visible: cupping and discontinuity at border (c) x2 and (d) x4 magnification data with edge extension [0 0.4]. Discontinuities seem better reconstructed but the quantitative aspect in reconstructed gray level is lost. (e) x2 and (e) x4 magnification data padded with x1 data [0.99 1.04] (f) x1 data enriched with details from x2 data using the proposed wavelet algorithm (g) x1 magnification data enriched with details from x4 data using the proposed wavelet algorithm [0.99 1.04]. Both methods yield qualitatively good reconstructions

sets are separated by a magnification factor 2, we can write the LR data set as

$$\tilde{p}_\theta^{(\Delta)}(r,z) = \int_{D_{\theta,r}} f(x,y,z)\,ds\ ,\ (r,z) \in [-L,L]^2 \quad (5)$$

which is discretized as

$$\tilde{p}_\theta(r_n, z_m)\ ,(r_n = n\Delta + r_0\ z_m = m\Delta + z_0),\quad 1 \le n \le N\ \ 1 \le m \le N \quad (6)$$

and the HR data as

$$p_\theta^{(\Delta/2)}(r,z) = \int_{D_{\theta,r}} f(x,y,z)\,ds\ \ (r,z) \in [-L/2, L/2]^2 \quad (7)$$

that is defined on half of the interval of p

$$p_\theta^{(\Delta/2)}(r_n, z_m)\ ,$$
$$(r_n = n\Delta/2 + r_0\ z_m = m\Delta/2 + z_0)\ \ 1 \le n \le N\ \ 1 \le m \le N \quad (8)$$

In pyramidal representation, we can write

$$p_\theta^{(\Delta/2)}(r_n, z_m) = p_\theta^{(\Delta)}(r_n, z_m) + d_\theta^{(\Delta)}(r_n, z_m)\ ,$$
$$(r_n, z_m) \in [-L/2, L/2]^2 \quad (9)$$

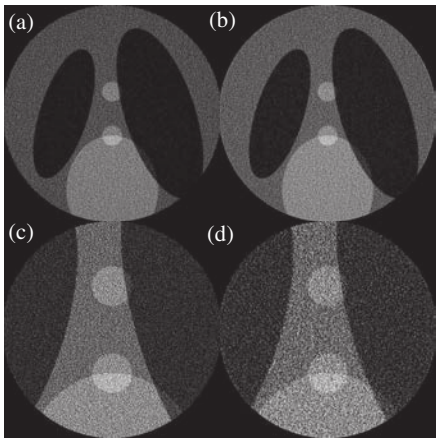

Fig. 4. Slices through the reconstructed volumes using noisy data, (0.1 % NSR) reconstructed with (a) x2 magnification data, edge extension (b) x2 magnification data padded with x1 data (c) x1 data enriched with details from x2 data using the proposed wavelet algorithm (d) x4 magnification data, edge extension (e) x4 magnification data padded with x1 data (f) x1 magnification data enriched with details from x4 data using the proposed wavelet algorithm.

To extend this relationship over the whole domain we introduce the approximate detail $\tilde{d}_\theta^{(\Delta)}(r_n, z_m)$ so that

$$p_\theta^{(\Delta/2)}(r_n, z_m) \approx p_\theta^{(\Delta)}(r_n, z_m) + \tilde{d}_\theta^{(\Delta)}(r_n, z_m), \quad (r_n, z_m) \in [-L, L] \times [-L, L] \tag{10}$$

with

$$\hat{d}_\theta^{(\Delta)}(r_n, z_m) = \begin{cases} d_\theta^{(\Delta)}(r_n, z_m), & (r_n, z_m) \in [-L/2, L/2]^2 \\ p_\theta^{(\Delta)}(r_n, z_m) * w(r_n, z_m), & (r_n, z_m) \in [-L/2, L/2]^2 \end{cases} \tag{11}$$

where w is an interpolation filter. The image at higher resolution can then be reconstructed using FBP. Combining (2) and (10) yields

$$f_R^{(\Delta/2)}(x, y, z) \approx f_R^{(\Delta)}(x, y, z) + g_R^{(\Delta)}(x, y, z) \tag{12}$$

with

$$g_R^{(\Delta)}(x, y, z) = \frac{1}{2} \int_0^\pi (\hat{d}_\theta^{(\Delta)} * h)(x_n \cos\theta + y_n \sin\theta, z_m)\, d\theta \,. \tag{13}$$

3. WAVELET ALGORITHM FOR ZOOM-IN TOMOGRAPHY

The above analysis assumes that the lower resolutions of p and are consistent. Should this not be the case, it is desired to use the lower resolutions from the LR data set on all the image, not just outside [*-L/2,L/2*]×[*-L/2,L/2*]. For this purpose we propose a wavelet algorithm for zoom-in tomography. It is based on the Haar wavelet due to its downsampling property, which seems an appropriate analogy to the multiresolution imaging setup.

One step of the 2D separable discrete wavelet transform of an image $p_\theta(n,m)$ consist in decomposing the image in one approximation $A_j p_\theta(n,m)$ and three details $D_j p_\theta(n,m)$ that can be written as

$$A_j p_\theta(n,m) \quad \sum_{k,l \in Z^2} h(k-2n)h(l-2m)A_{-1} p_\theta(k,l)$$

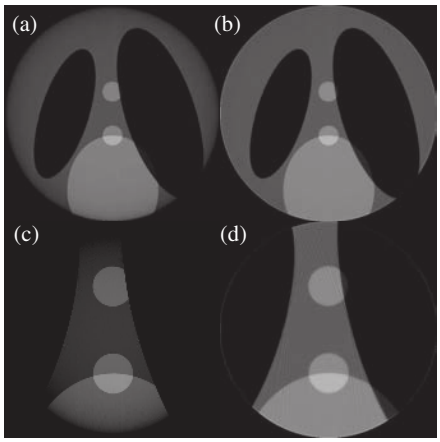

Fig. 5. Slices through the reconstructed volumes using data where a random offset has been introduced to the high resolution data, reconstructed with (a) x2 magnification data padded with x1 data (b) x1 data enriched with details from x2 data using the proposed wavelet algorithm (c) x4 magnification data padded with x1 data (d) x1 magnification data enriched with details from x4 data using the proposed wavelet algorithm.

$$D_j^i p_\theta(n,m) = \sum_{k,l \in Z^2} w^i(k-2n, l-2m) A_{j-1} p_\theta(k,l)$$

$$w^1(k,l) = h(k)g(l) \quad w^2(k,l) = g(k)h(l) \quad w^3(k,l) = g(k)g(l) \tag{14}$$

Where h(k) and g(l) are the respective low and high pass filters used in the decomposition. For a suitable choice of these filters, the decomposition may be inverted as:

$$A_{j-1} p_\theta(n,m) = \sum_{k,l \in Z^2} \tilde{h}(k-2n, l-2m) A_j p_\theta(n,m) + \sum_{i=1}^{3} \sum_{k,l \in Z^2} \tilde{w}^i(k-2n, l-2m) D_j^i p_\theta(n,m)$$

$$A_0 p_\theta(n,m) = \sum_{k,l \in Z^2} \tilde{h}(k-2n, l-2m) A_1 p_\theta(n,m) + \sum_{i=1}^{3} \sum_{k,l \in Z^2} \tilde{w}^i(k-2n, l-2m) D_1^i p_\theta(n,m) \tag{15}$$

We begin by observing that, ideally, the HR data only differs from the LR data in that, apart from being truncated, it contains information at one higher scale. The HR projection is transformed to the first level using (14). The approximation coefficients $A_j P\theta$ are then swapped for the recorded LR image and the details zero-padded so that they are kept at the same size as the LR imqge. This composite transform is then inverse transformed using (15) to achieve a non-truncated projection that contains the low frequencies from the LR scan across the whole image and the high frequencies from the HR scan in the ROI.

4. COMPUTER SIMULATION

We evaluate four methods for zoom-in tomography on the 3D Shepp-Logan phantom: zero padding of the projections, edge extension, padding with a supersampled version of the LR data using Fourier interpolation and finally the proposed method. Three different data sets were used. A complete data set is generated

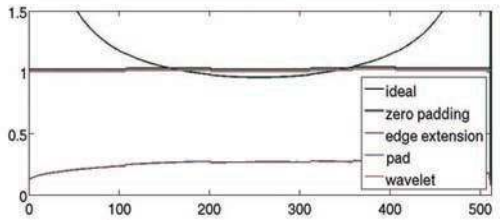

Fig. 6, Profile plots of the center line of each reconstruction at the x4 magnification level with noise-free data. Note the strong cupping artifact in the reconstructions with zero padding and edge extension. The wavelet and padding reconstructions give very similar results

through analytical projections; at an image size of 2048×2048 over 768 projections. A complete data set (corresponding to 1x magnification) was generated by downsampling the initial data set to 512×512. The x2 magnification data set was generated by downsampling the initial data set to 1024×1024 and truncating from both sides to 512×512, and the x4 magnification data was created by truncating the initial data set to 512×512 (Fig. 2). Data was also generated with additive noise at different noise levels, as well as data where different offsets where added to the HR scan.

5. RESULTS

In Fig. 3, reconstructions using noise-free data is shown. Note the strong cupping artifacts in the zero padded data. This is slightly better in the edge extended reconstruction, but it is still far from quantitative. The reconstructions using two resolutions directly by padding and the proposed method however yields reconstructions seemingly very close to the ideal. These observations are verified in profile plots (Fig. 6) and on measurements of the NRMSE shown in Tab. 1.

Looking at results from noisy data (Fig. 4), the quantitative aspect seems preserved, but the noise structure appears different. Considering the error at different noise levels (Fig. 7a), the wavelet method seems more sensitive to noise. This could possibly be alleviated, however, by the possibility of including denoising in the algorithm by shrinkage of the detail coefficients.

Finally, reconstruction of data with an introduced offset seems to induce a cupping artifact in the padding algorithm, whereas reconstruction with the wavelet algorithm seems insensitive to the offset (Fig. 5). This is verified by looking at the reconstruction over different offset levels; where the wavelet reconstruction; as conjectured; remains unaffected (Fig. 7b).

5. DISCUSSION AND CONCLUSIONS

In this work; we addressed the problem of quantitative reconstruction from truncated projections when a supplementary low resolution; non-truncated data set is available. We formalized the problem of 3D parallel beam zoom-in reconstruction in the multiresolution framework and proposed a wavelet based

TABLE I
RECONSTRUCTION ERROR USING NOISE-FREE DATA

Reconstruction	NRMSE (%)
Edge extension, x2	67.7
Padding, x1 & x2	1.62
Wavelet, x1 & x2	1.61
Edge extension, x4	80.7
Padding, x1 & x4	1.57
Wavelet, x1 & x4	1.56

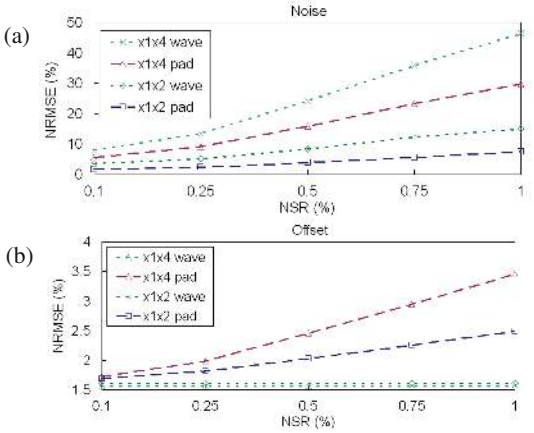

Fig. 7: Error plots from reconstructions using the different methods and data sets. (a) Additive, Gaussian white noise. The wavelet method seems slightly more sensitive. (b) A small offset introduced between the two acquisitions. As conjectured, the wavelet method is insensitive to this type of errors.

algorithm for reconstruction. The algorithm is tractable to process very large data set such as provided by recent μCT systems. The proposed algorithm showed slightly better reconstruction for noise-free data, slightly worse noise performance than Fourier interpolation, and is insensitive to offsets between the two data sets. Further studies are necessary to study the best choice of wavelet filters, the optimal acquisition conditions in terms of number of projections and signal to noise ratio. In future work the proposed method will be applied to experimental data acquired on a parallel beam 3D SR μCT setup. This will also raise the problem of registrating the two data sets acquired at different magnifications.

6. REFERENCES

[1] F. Natterer, *The Mathematics of Computed Tomography*, SIAM, 2001.

[2] H. Kudo, M. Courdurier, F. Noo, and M. Defrise, "Tiny *A Priori* Knowledge Solves the Interior Problem in Computed Tomography," *Phys. Med. Biol.* Vol. 53, pp. 2207-2231, 2008.

[3] K. Hiroshi, and A. Noboru, "An Iterative Reconstruction from Truncated Projection Data," *IEEE Trans. Nucl. Sci.* Vol. 32, pp. 1217-1224, 1985.

[4] F. Peyrin, M. Zaim, and R. Goutte, Construction of Wavelet Decompositions for Tomographic Images, J. *Math. Imaging Vis.* Vol. 3, pp. 105-121, 1993.

[5] T. Olson and J. DeStefano, "Wavelet Localization of the Radon Transform," *IEEE Trans. Sig. Proc.* Vol. 42, pp. 2055-2067, 1994.

[6] S. Bonnet, F. Peyrin, F. Turjman, and R. Prost, "Tomographic Reconstruction using Nonseparable Wavelets", *IEEE Trans. Im. Proc.* Vol 9, pp. 1445-1450, 2000.

[7] O. Nalcioglu, Z. H. Cho, and R. Y. Lou, "Limited Field of View Reconstruction in Computerized Tomography," *IEEE Trans. Nucl. Sci.* Vol. NS-26, pp. 546-551, 1979.

[8] D. J. Gentle and N. M. Spyrou, "Region of interest tomography in industrial applications," *Nucl. Instr. Meth. Phys. Res. A*, Vol. 299, pp. 534-537, 1990.

[9] X. Xiao, F. De Carlo, and S. R. Stock, "X-ray Zoom-in Tomography of Calcified Tissue," *Proc. SPIE* Vol. 7078, pp. 707810, 2008.